

## A core-substituted naphthalene diimide based supramolecular triangle and its self-assembly into nanostructures

Samantha T. Aragon,<sup>a</sup> Edgar U. Lopez-Torres<sup>b</sup>, Franchesca C. Tinacba,<sup>a</sup> Camille J. Kwan,<sup>a</sup> Joshua J. Do,<sup>a</sup> Rosanna Jeas,<sup>a</sup> Daniella S.A. Unpingco,<sup>a</sup> Daniel J. Wherritt,<sup>c</sup> Jon R. Parquette<sup>\*b</sup>, Peter J. Cragg <sup>\*d</sup> and Erendra Manandhar <sup>\*a</sup>

- a) Department of Chemistry and Biochemistry, St. Mary's University, San Antonio, TX, US
- b) Department of Chemistry and Biochemistry, Ohio State University, Columbus, OH, US.
- c) Department of Chemistry, University of Texas at San Antonio, San Antonio, US
- d) School of Applied Sciences, University of Brighton, Brighton, UK

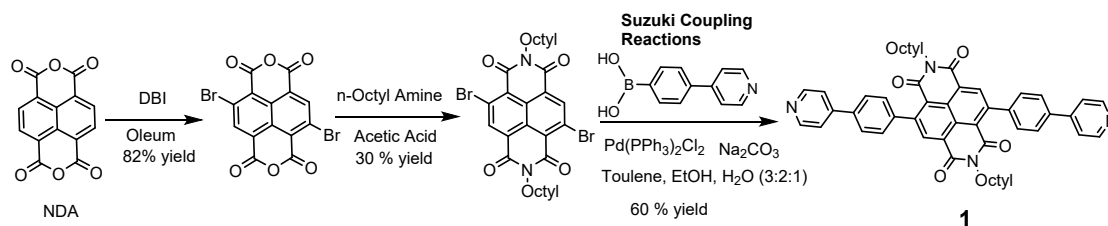
### Supplementary Material:

#### Table of Contents:

General technique	1
Synthesis	2-3
<sup>1</sup> H and <sup>31</sup> P NMR	4-6
<sup>1</sup> H and <sup>31</sup> P NMR Stack plot	7-8
High resolution mass spectrometry	9-11
Computational Detail	12-13
AFM and TEM Imaging	14-15
UV-Vis study	16
Cyclic Voltammetry	17-18
1D and 2D NMR	18-24
References	25

**General techniques:** One- and two-dimensional NMR spectra were recorded on High field 500 MHz Bruker ADVANCE III HD Nuclear Magnetic Resonance Spectrometer in the appropriate deuterated solvents. Chemical shifts are reported in parts per million (ppm) downfield from tetramethylsilane (0 ppm) as the internal standard and coupling constants ( $J$ ) are recorded in hertz (Hz). The multiplicities in the <sup>1</sup>H NMR spectra are reported as (br) broad, (s) singlet, (d) doublet, (dd) doublet of doublets, (ddd) doublet of doublet of doublets, (t) triplet, (sp) septet and (m) multiplet. All spectra are recorded at ambient temperature. UV-Vis experiments were performed on SHIMADZU UV/Vis Spectrophotometer. Fluorescence experiments were carried out on HORIBA Scientific Fluorolog Spectrofluorometer. IR spectra were recorded on a Bruker Tensor 27 Fourier Transform Infrared Spectrometer with diamond ATR. The characteristic functional groups are reported in wavenumbers (cm<sup>-1</sup>), and are described as weak (w), medium (m), strong (s) and very strong (vs). Cyclic Voltammetry experiments were performed on a VersaStudio electrochemistry system at 298K using a 2mm diameter gold electrode, a platinum wire auxiliary electrode, and Ag/AgNO<sub>3</sub> reference electrode. The gold electrode was rinsed and dried with water and methanol after polishing with 0.05 μM alumina immediately prior to use. A 0.05 M tetrabutylammonium perchlorate is used as supporting electrolyte.

## Synthesis



## Synthesis

2,6-dibromo-1,4,5,8-naphthalene tetracarboxylic dianhydride and *N, N'*-dioctyl-2,6-dibromo-1,4,5,8-naphthalene tetracarboxylic diimide were prepared according to literature procedures.<sup>1</sup>  $(Et_3P)_2Pt \cdot 2OTf$ ,  $Pt(dppp) \cdot 2OTf$  and  $Pd(dppp) \cdot 2OTf$  were prepared following reported procedures.<sup>2,3</sup>

### *N, N'*-dioctyl-2,6-bis (pyridinyl phenyl)-1,4,5,8- Naphthalene tetracarboxylic diimide (**1**)<sup>4</sup>

A 500 mL flask was charged with 2,6-dibromo-1,4,5,8-naphthalene tetracarboxylic dianhydride (1.34 g, 2.07 mmol), 4-Pyridinyl phenyl boronic acid (1.23 g, 6.21 mmol),  $Pd(PPh_3)_2Cl_2$  (0.308 g, 0.440 mmol),  $Na_2CO_3$  (2.34 g, 22.0 mmol), and toluene/methanol/water (50 mL/30 mL/20 mL). The reaction mixture was then heated at 110°C under nitrogen for two days with stirring. After cooling down to room temperature, water was added and organic layer separated. The aqueous solution was further extracted with dichloromethane (3 × 50 mL). The combined organic layers were washed with brine (100 mL), dried over  $MgSO_4$ , and evaporated to dryness under vacuum. The residue was purified by silica gel chromatography (chloroform /hexane, 9/1), to afford 1.24 g (1.55 mmol) of compound **1** as a yellow solid in 75% yield.

**<sup>1</sup>H NMR (300 K,  $CDCl_3$ , 500MHz):**  $\delta$ 8.74 (d,  $J=5.4$  Hz 4H), 8.71 (s, 2H), 7.84 (d,  $J=8.0$  Hz 4H), 7.65 (d,  $J=5.9$ Hz, 4H), 7.57 (d,  $J=8.6$ Hz, 4H), 4.11 (t,  $J=7.9$ Hz, 3H), 1.68 (m, 4H), 1.24-1.38 (m, 20H), 0.89 (t,  $J=7.0$ Hz, 6H),

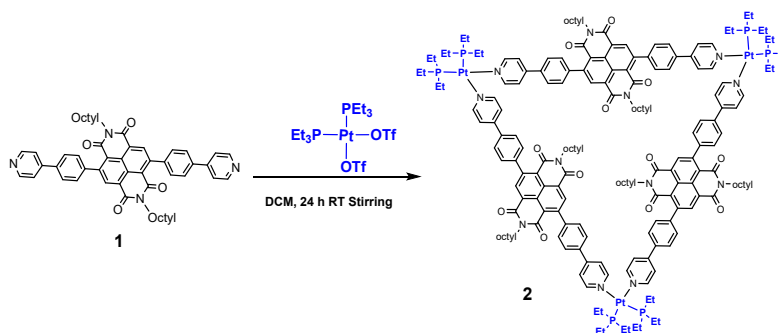
**<sup>13</sup>C NMR (300 K,  $CDCl_3$ , 500MHz):**  $\delta$ 162.36, 150.40, 147.63, 146.96, 141.37, 138.00, 135.75, 128.97, 127.35, 127.08, 125.78, 123.02, 121.65, 41.12, 31.77, 29.29, 29.20, 28.04, 27.06, 22.62, 14.08

**IR (ATR solid):** 2952  $\nu_{C-H}$  (w), 2927  $\nu_{C-H}$  (w), 2854  $\nu_{C-H}$  (w), 1703  $\nu_{C=O}$  (m), 1666  $\nu_{C=C}$  (s)  $cm^{-1}$ .

**HRMS** calculated for  $C_{52}H_{53}N_4O_4$   $[M+H]^+$ : 797.4061 and found 797.4048

$C_{52}H_{53}N_4O_4$   $[M+2H]^{2+}$ : 399.2067 and found 399.2066

## Self-assembly of **2**<sup>3</sup>



A mixture of  $(\text{Et}_3\text{P})_2\text{Pt} \cdot 2\text{OTf}$  (29.18 mg, 0.04 mmol) and **1** (31.88 mg, 0.04 mmol) in a dry dichloromethane (20.0 mL) was stirred under nitrogen at room temperature for 48 h. The solution was filtered to remove any insoluble particles and reduced to half by degassing nitrogen gas. A slow vapor diffusion of diethyl ether into the solution over 24 h yielded a yellow solid which was collected by centrifugation, washed twice with diethyl ether (10 ml) and dried in vacuum to give the final product (146 mg, 0.032 mmol, 80% yield).

**$^1\text{H}$  NMR (300 K,  $\text{CDCl}_3$ , 500MHz):**  $\delta$ 9.46(d,  $J=5.5$  Hz 12H), 8.60 (s, 6H), 7.94 (d,  $J=6.0$  Hz 12H), 7.89 (d,  $J=8.0$ Hz, 12H), 7.53 (d,  $J=8.0$ Hz, 12H), 4.03 (t,  $J=7.2$  & 7.8 Hz, 12H), 1.94 (q,  $J=8.0$ , Hz, 36H), 1.59 (m, 12H), 1.39 (m, 54H), 1.16 (m, 26H), 1.27 (m, 34H), 0.77 (t,  $J=7.0$ Hz, 18H),

**$^{13}\text{C}$  NMR (300 K,  $\text{CDCl}_3$ , 500MHz):**  $\delta$ 162.04, 151.40, 146.37, 143.70, 135.14, 133.94, 129.17, 127.31, 125.82, 124.68, 123.11, 118.43, 41.09, 31.70, 29.24, 29.13, 78.96, 26.98, 22.56, 15.83, 14.03, 7.82

**IR (ATR solid):** 2926  $\nu_{\text{C-H}}$  (w), 2859  $\nu_{\text{C-H}}$  (w), 1704  $\nu_{\text{C=O}}$  (m), 1662  $\nu_{\text{C=C}}$  (m)  $\text{cm}^{-1}$ .

**ESI-MS:** 614.2723 ( $[\text{2-6OTf}]^{6+}$ ), 766.7163 ( $[\text{2-5OTf}]^{5+}$ ), 995.6369 ( $[\text{2-4OTf}]^{4+}$ )

**Self-assembly with  $\text{Pt}(\text{dppp}) \cdot 2\text{OTf}$  and  $\text{Pd}(\text{dppp}) \cdot 2\text{OTf}$ :** It is carried out in a similar way as with  $(\text{Et}_3\text{P})_2\text{Pt} \cdot 2\text{OTf}$ .

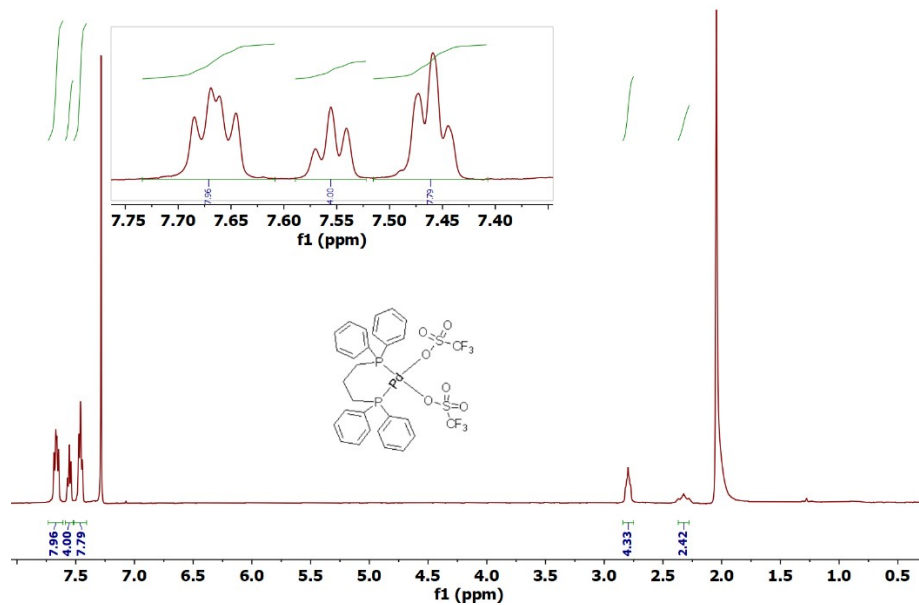


Figure S1 :  $^1\text{H}$  NMR of  $\text{Pd}(\text{dppt})\cdot 2\text{OTf}$  in  $\text{CDCl}_3$ .

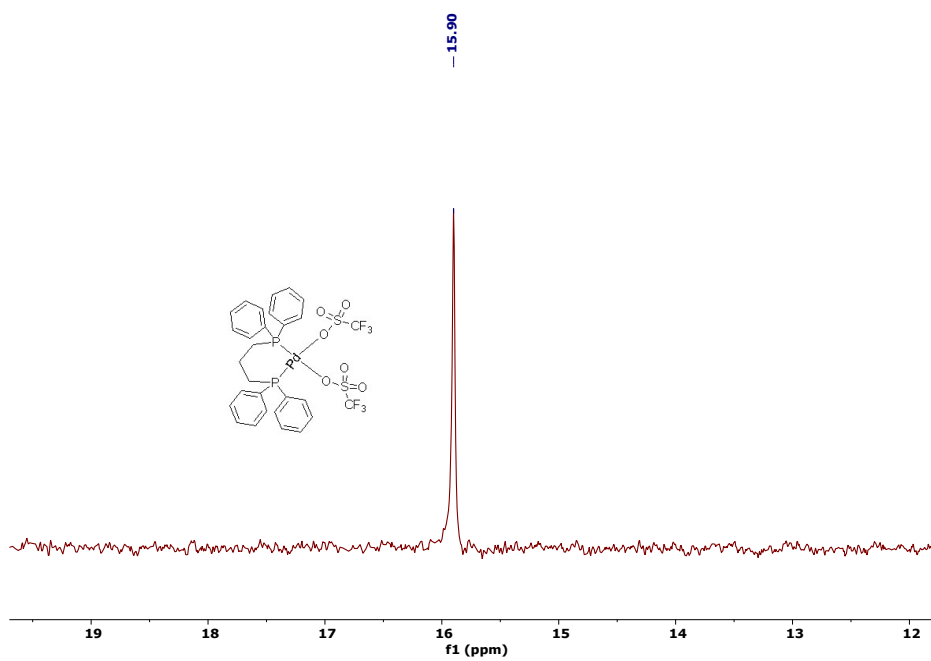


Figure S2 :  $^{31}\text{P}$  NMR of  $\text{Pd}(\text{dppt})\cdot 2\text{OTf}$  in  $\text{CDCl}_3$ .

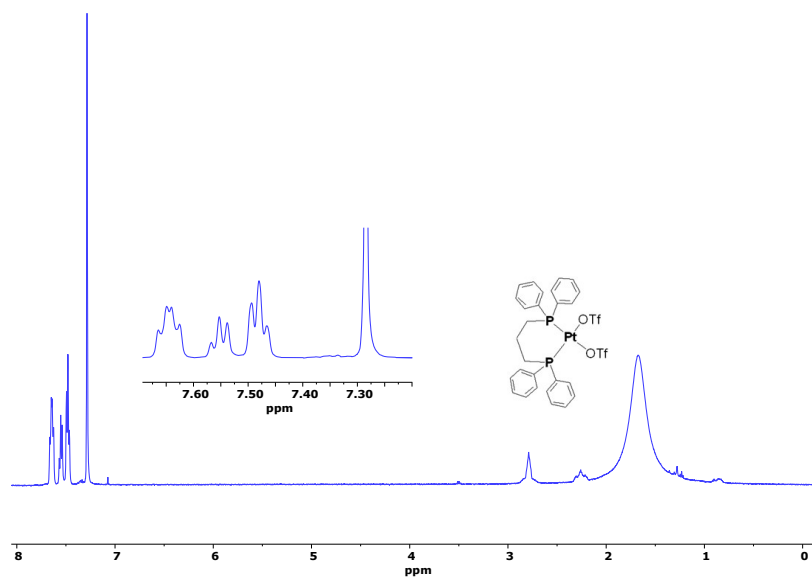


Figure S3 :  $^1\text{H}$  NMR of  $\text{Pt}(\text{dppt})\cdot 2\text{OTf}$  in  $\text{CDCl}_3$ .

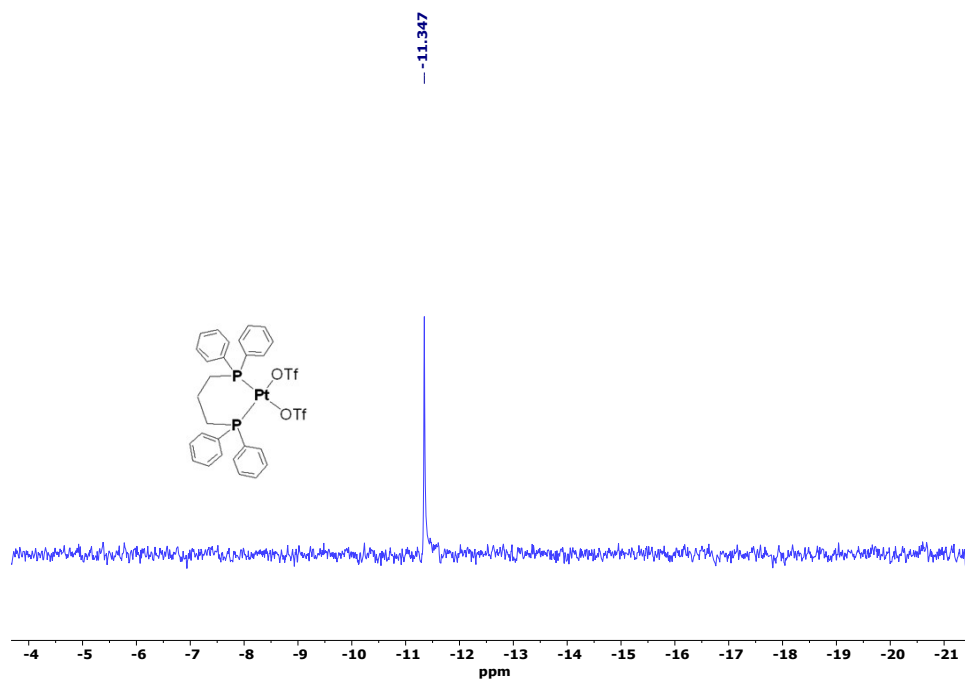


Figure S4 :  $^{31}\text{P}$  NMR of  $\text{Pt}(\text{dppt})\cdot 2\text{OTf}$  in  $\text{CDCl}_3$ .

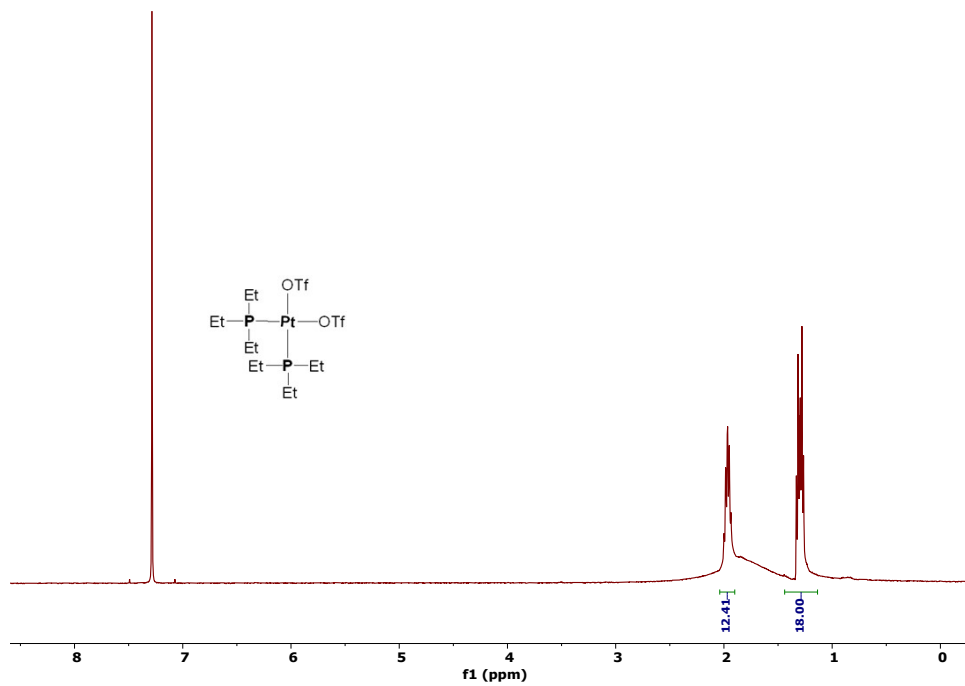


Figure S5 :  $^1\text{H}$  NMR of  $(\text{Et}_3\text{P})_2\text{Pt} \cdot 2\text{OTf}$  in  $\text{CDCl}_3$ .

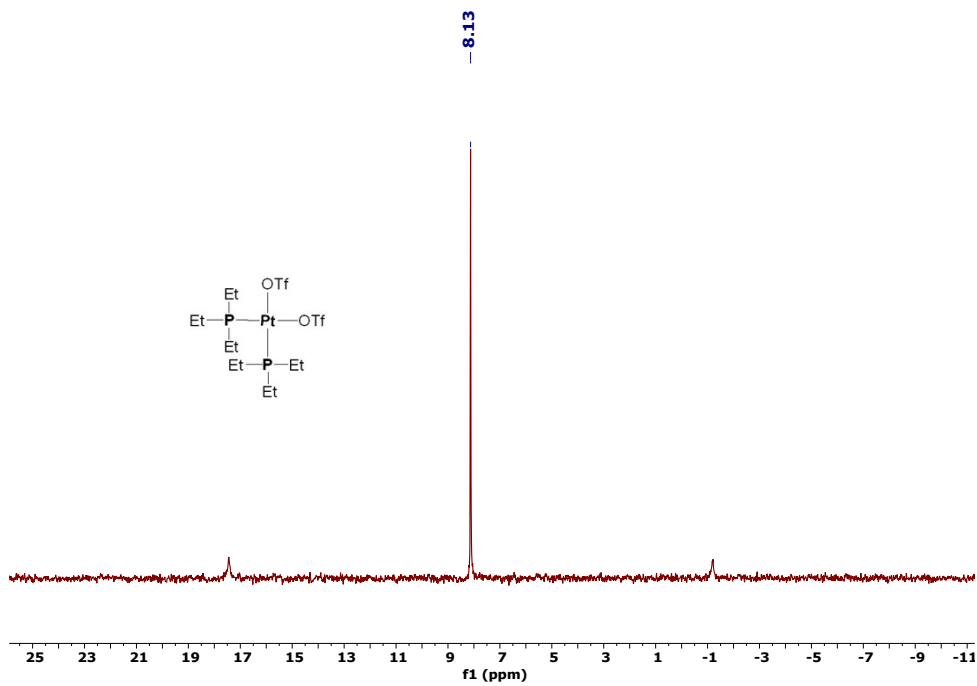


Figure S6 :  $^{31}\text{P}$  NMR of  $(\text{Et}_3\text{P})_2\text{Pt} \cdot 2\text{OTf}$  in  $\text{CDCl}_3$ .

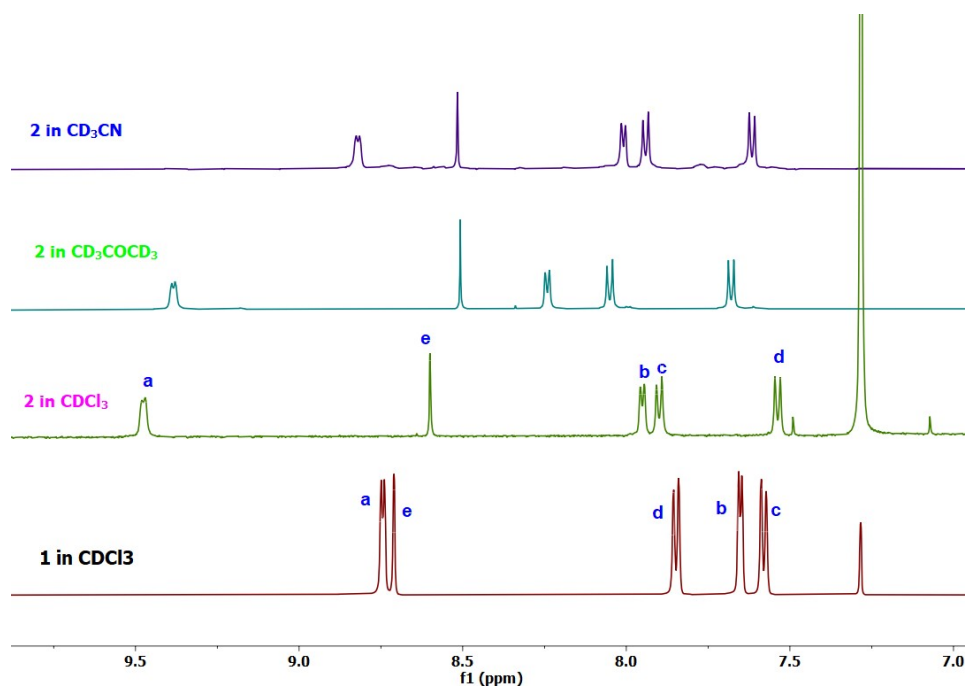


Figure S7 :  $^1\text{H}$  NMR stack plot of **1** and **2** in various solvents.

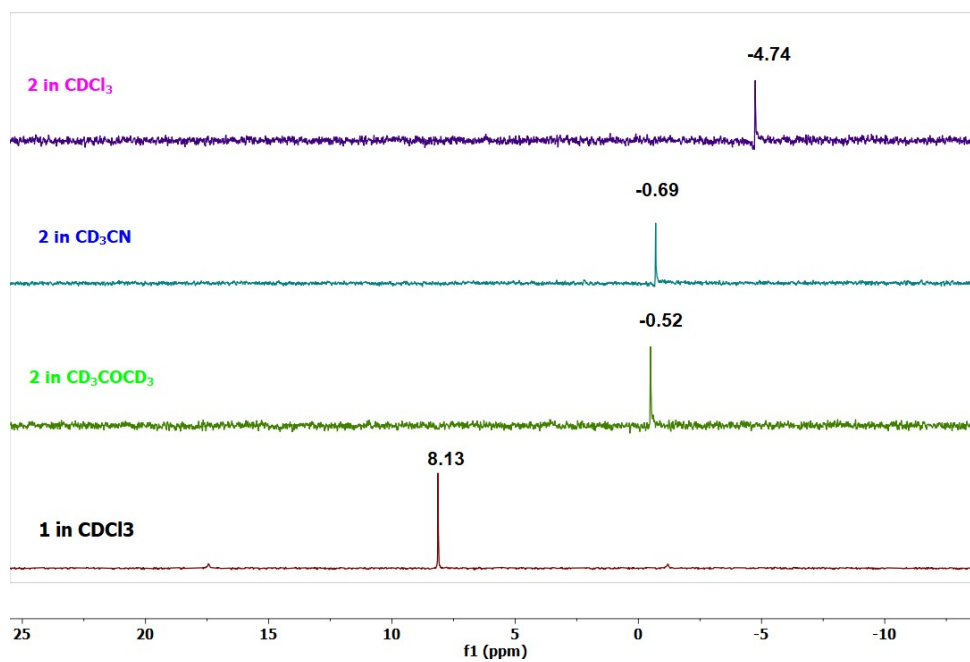


Figure S8 :  $^{31}\text{P}$  NMR stack plot of **1** and **2** in various solvents.

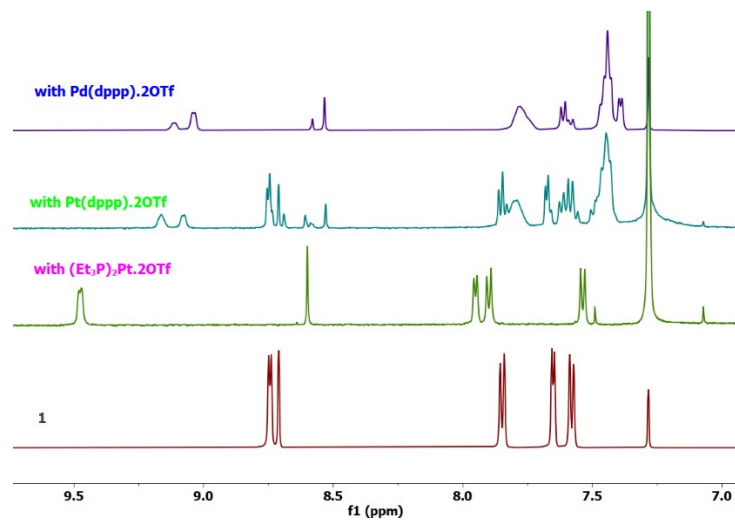


Figure S9:  $^1\text{H}$  NMR stack plot of **1** and with  $(\text{Et}_3\text{P})_2\text{Pt} \cdot 2\text{OTf}$ ,  $\text{Pt}(\text{dppp}) \cdot 2\text{OTf}$  and  $\text{Pt}(\text{dppp}) \cdot 2\text{OTf}$  in  $\text{CDCl}_3$ .

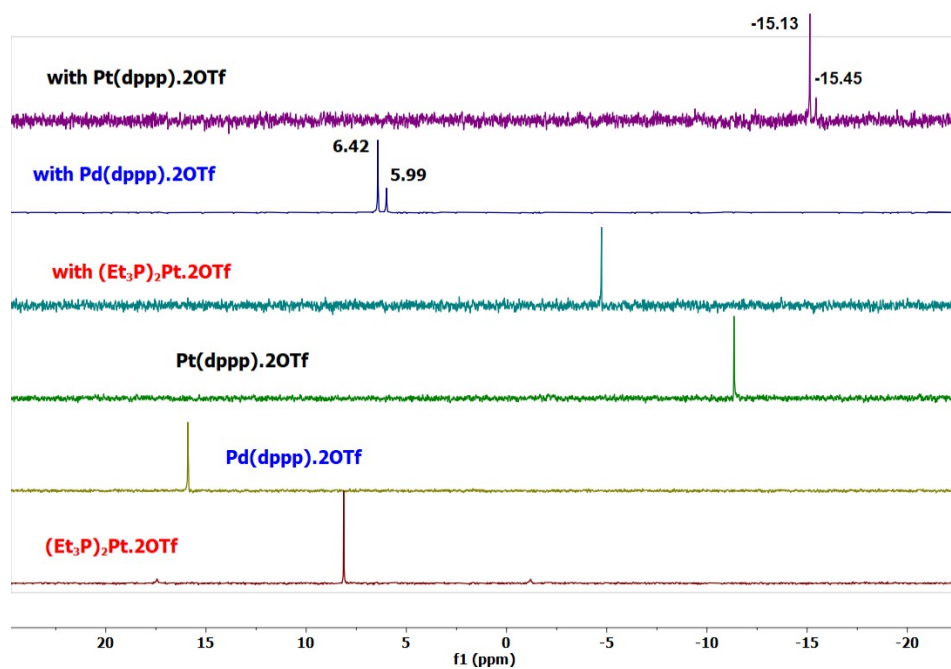


Figure S10:  $^{31}\text{P}$  NMR stack plot of  $(\text{Et}_3\text{P})_2\text{Pt} \cdot 2\text{OTf}$ ,  $\text{Pt}(\text{dppp}) \cdot 2\text{OTf}$  and  $\text{Pt}(\text{dppp}) \cdot 2\text{OTf}$  and its complex with **1** in  $\text{CDCl}_3$ .

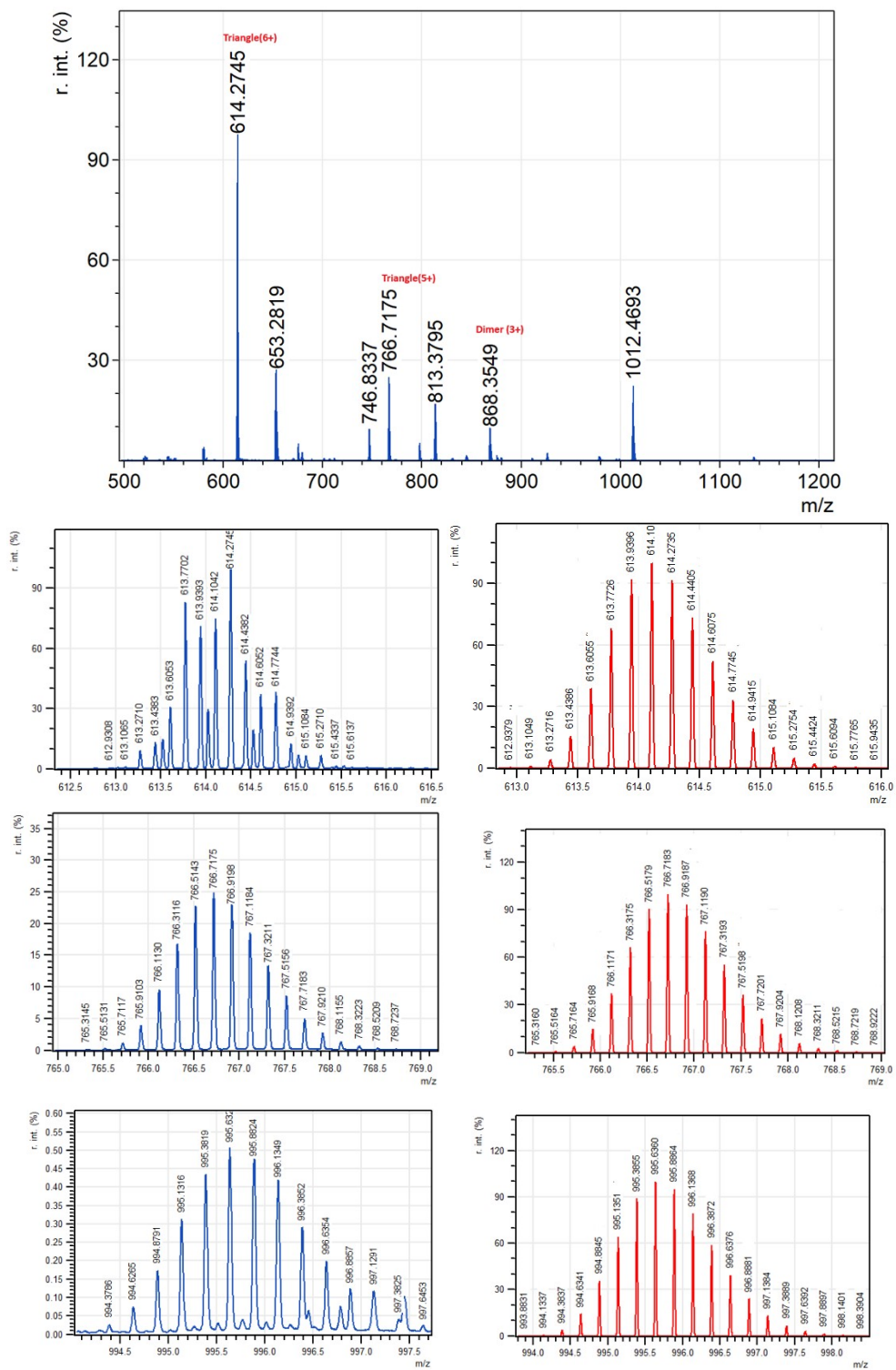


Figure S11: ESI mass spec of **2** with experimental (blue) and theoretical (red) isotopic distribution of peaks m/z.

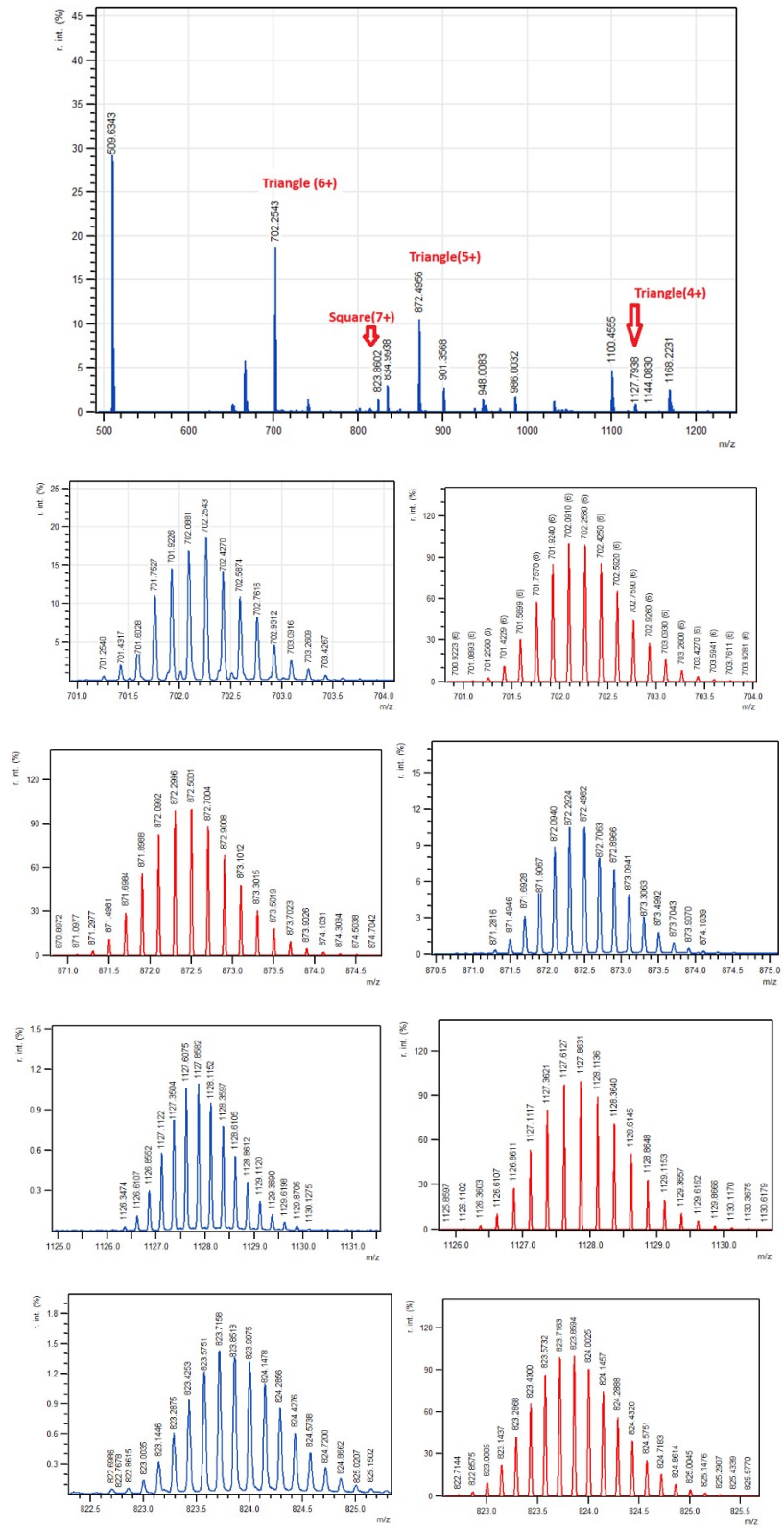


Figure S12: ESI mass spec of Pt(dppp) capped complex with experimental (blue) and theoretical (red) isotopic distribution of peaks m/z.

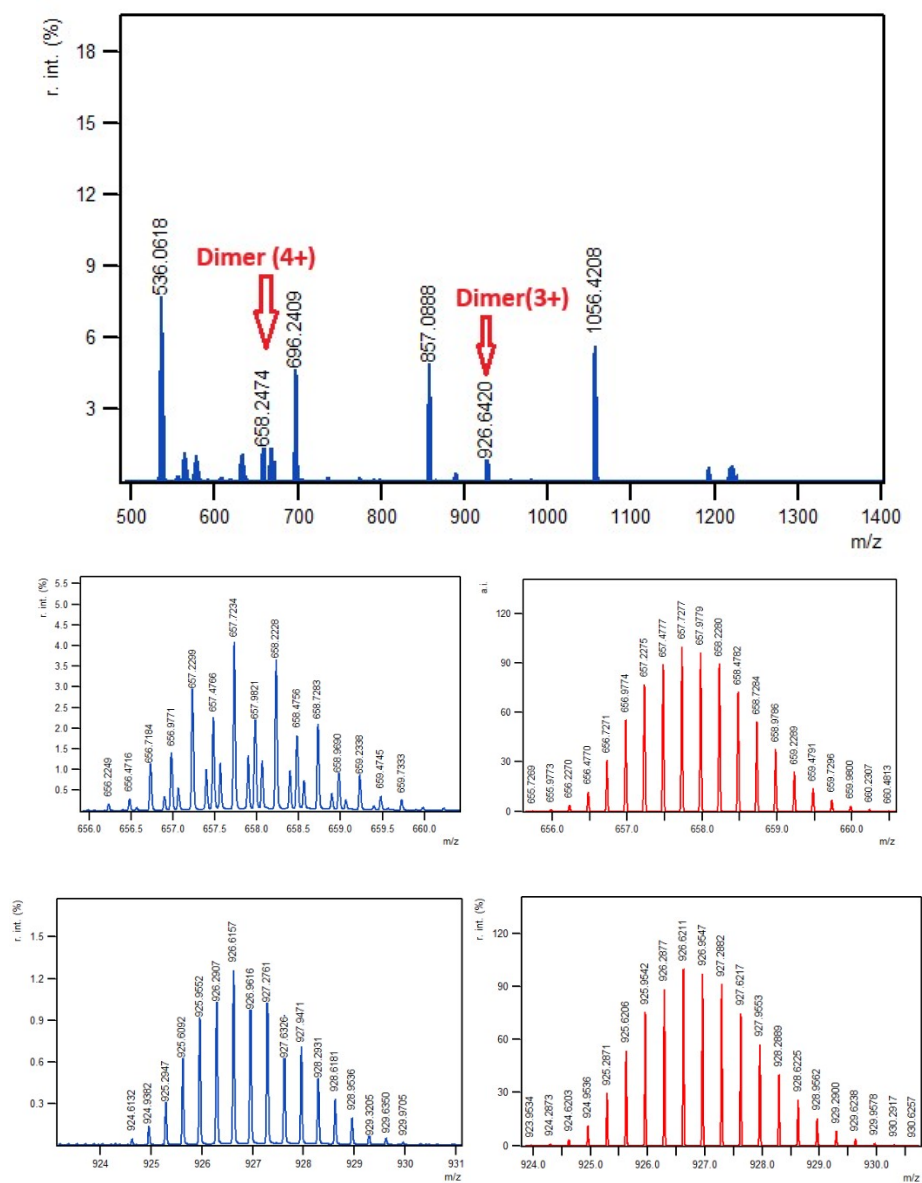


Figure S13: ESI mass spec of Pd(dppp) capped complex with experimental (blue) and theoretical (red) isotopic distribution of peaks m/z.

## Computational Experimental

Calculations were carried out using *Spartan '24*.<sup>5</sup> Using the *Build* option, ligand **1** was created and molecular mechanics methods (MMFF) were used to generate the lowest energy gas phase geometry. This structure was used to create the trimeric metallocycle **2** which was also subject to geometry optimisation by molecular mechanics. Ligand **1** was further investigated by density functional methods (DFT/B3LYP/6-31G\*) to generate orbital energies of -6.40 eV (HOMO) and -3.43 eV (LUMO).

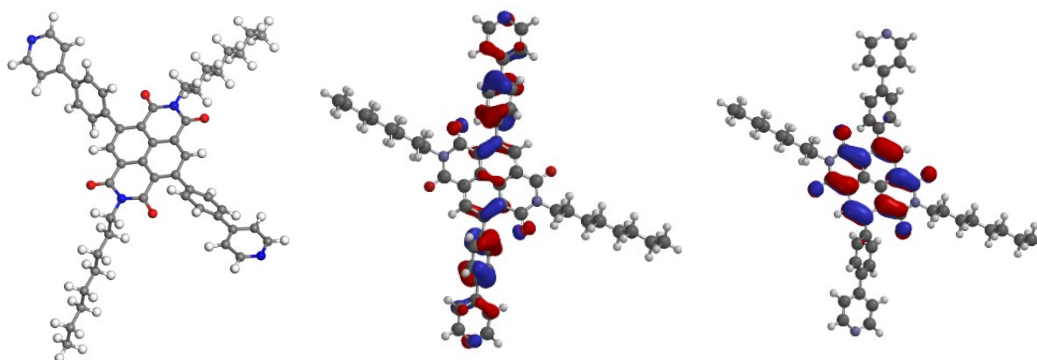


Figure S14: DFT optimized structure, HOMO and LUMO of the ligand **1**.

Due to the number of atoms involved, complex **2** was modelled by semiempirical methods (PM6) in the gas phase using an approach developed for macrocycles.<sup>6</sup>

### Effect of triflate on **1**

NDIs are known to form anion- $\pi$  adducts<sup>7</sup> and, indeed when modelled at a simple molecular mechanic's level, it appears that two triflates can approach from either face of the **1** with two oxygen atoms of each pointing to its surface. However, on more rigorous investigation (DFT/BLY3P/6-31G\*), the anions relocated to the periphery of **1**.

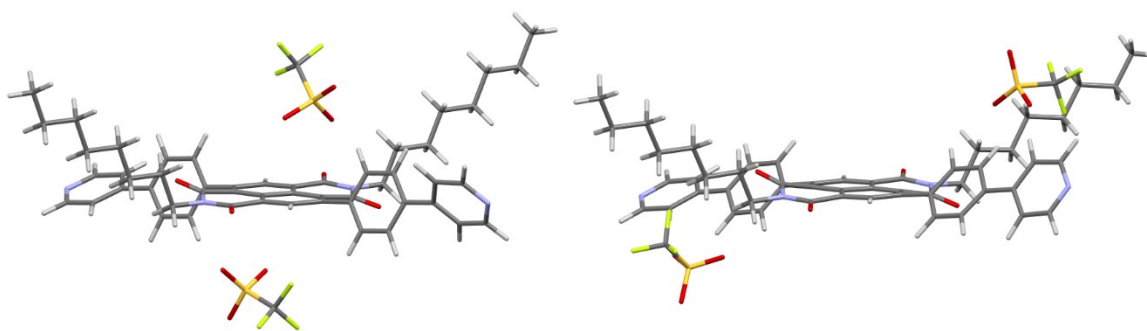


Figure S15: Geometry of **1**·(OTf)<sub>2</sub> optimized by molecular mechanics (left) and DFT (right).

### Effect of triflate on 2

Similarly, a molecular mechanics geometry optimized calculation of **2** was carried out with six triflate anions to determine any effect of triflate anions on complex structure. Very little structural difference was found. All parameters such as bond angles and distances are almost same in both structures showing virtually no effect of triflate anions in the structure.

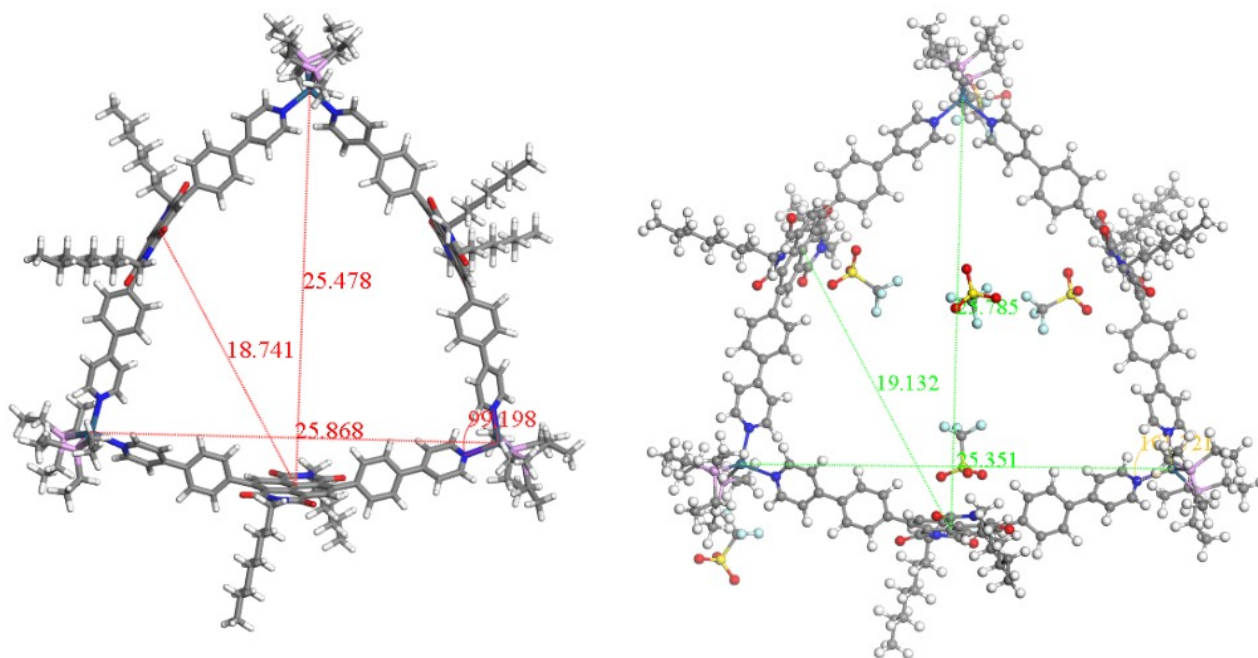


Figure S16: Original structure (left) and structure after minimizing with six triflate anions (right).

## AFM and TEM Imaging

Atomic force microscopy (AFM) was performed in ScanAsyst mode using a Bruker AXS Dimension Icon AFM equipped with a ScanAsyst-Air probe. The AFM images were collected with Bruker silicon tips (0.2-0.8N/m) with a silicon nitride cantilever. The sample was prepared by depositing it onto a freshly cleaved mica surface, followed by washing with deionized water and drying prior to imaging. Images were acquired at a resolution of 512 x 512 pixels with a scan rate of 0.9–1 Hz. Data analysis was conducted with Bruker NanoScope Analysis 3.0 software. Transmission Electron Microscopy (TEM): Samples were diluted and dropped on carbon-coated copper grids (Ted Pella, Inc.) for 1 min. Excess solution was wicked off, and the sample grid was negatively stained with 2% (w/w) uranyl acetate solution for 45 s. The dried specimen was observed with Technai G2 Spirit TEM instrument operating at 80 keV. Images were analyzed with ImageJ imaging software.

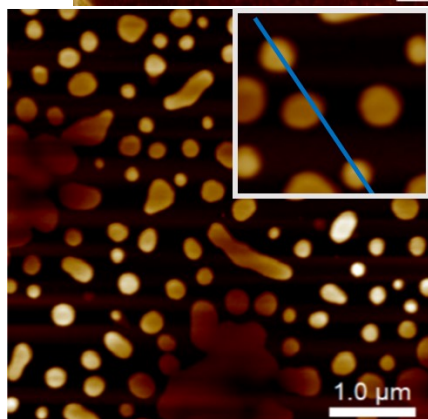
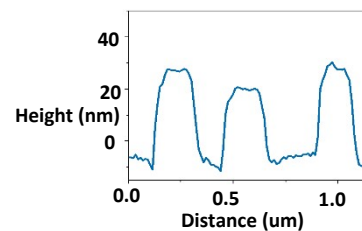
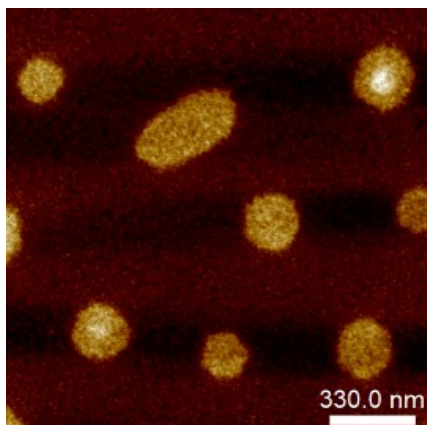
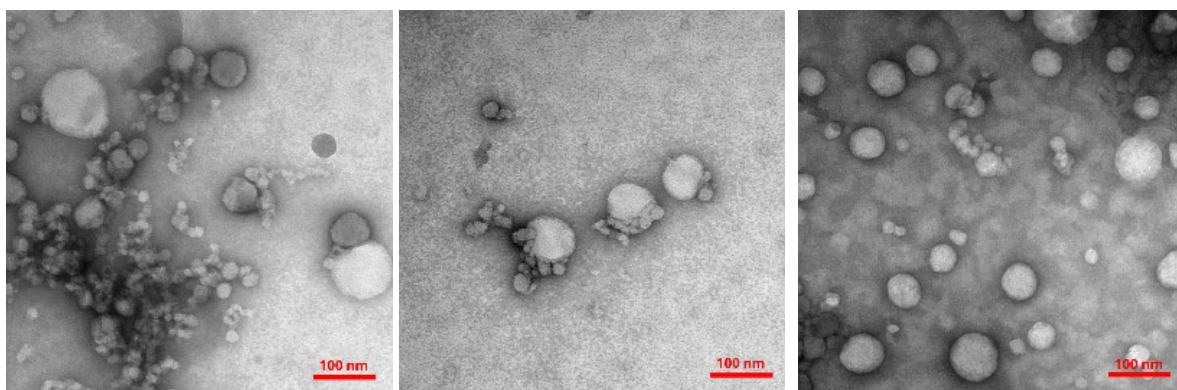


Figure *S17*: AFM and TEM images of **2** (0.5 mM) in CH<sub>3</sub>CN. A section analysis showing AFM height measurement with the height generated by the nano particles along the blue lines in the image.

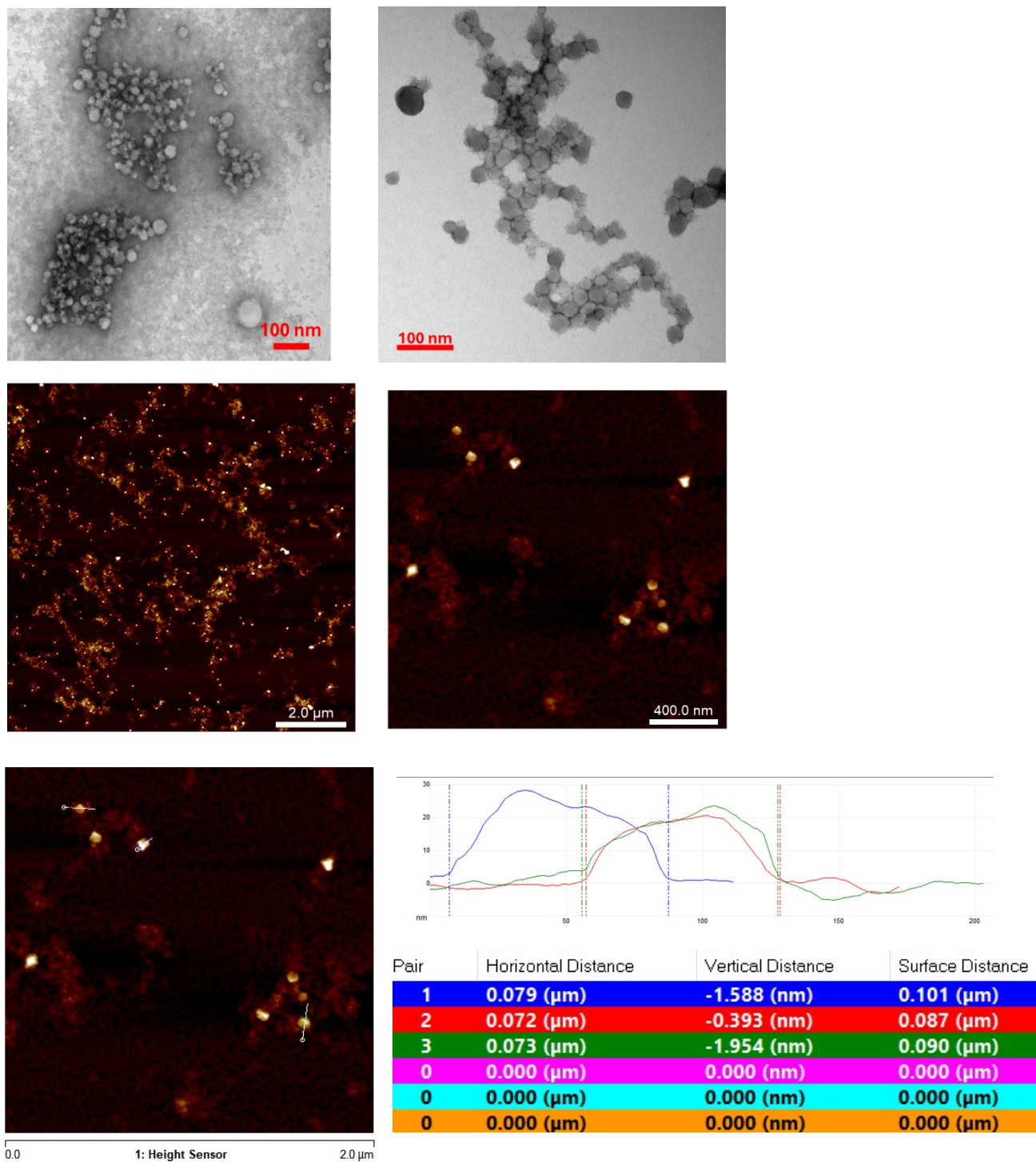


Figure S18: AFM, section analysis and TEM images of **2** (5.0 mM) in CH<sub>3</sub>CN.

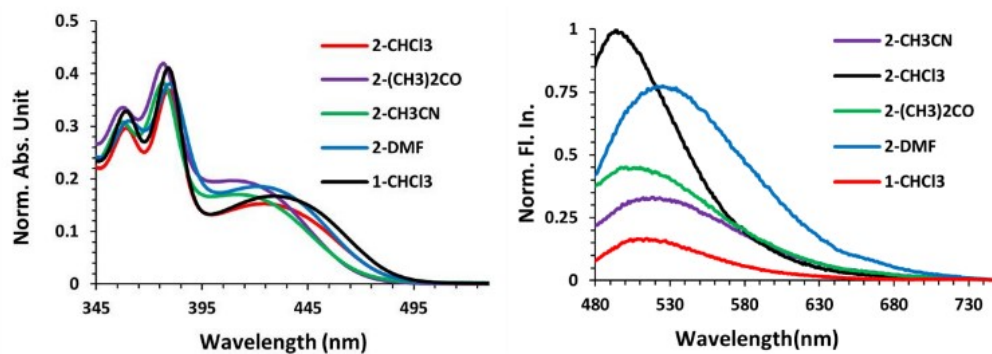


Figure S19: (a) Absorption spectra of **1** (20 μM) in CHCl<sub>3</sub> and **2** in various solvents. (b) Fluorescence spectra of **1** (20 μM) in CHCl<sub>3</sub> and **2** (20 μM) in various solvents.

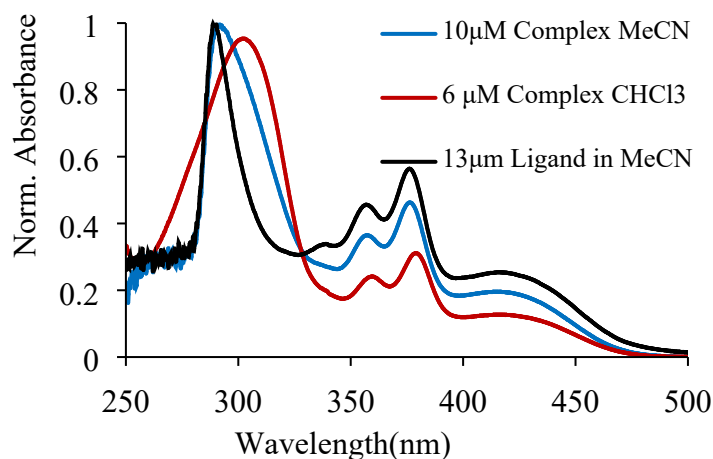


Figure S20: UV-Vis absorbance of **1** in CHCl<sub>3</sub> and **2** in CHCl<sub>3</sub> and CH<sub>3</sub>CN.

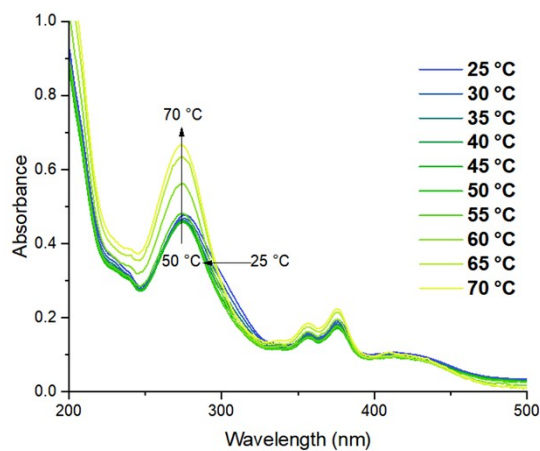


Figure S21: UV-Vis absorption spectra of **2** (30.0 μM) in CH<sub>3</sub>CN with different temperature from 25 °C to 70 °C. (Solution was equilibrated for 5.0 minute prior to each scan)

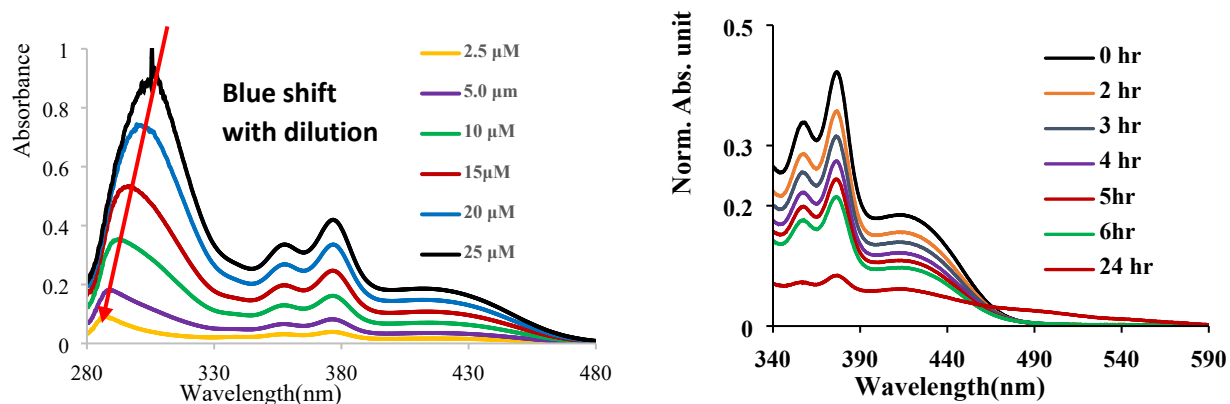


Figure S22: UV-Vis absorption spectra of **2** in CH<sub>3</sub>CN with different concentration from 2.5 μM to 25 μM at room temperature (left) and UV-Vis absorption of **2** in CH<sub>3</sub>CN as a function of time.

Name	Mean	Standard Deviation	RSD	Minimum	Maximum
Z-Average (nm)	5064.65	354.729	7.004	4691.383	5397.353
Polydispersity Index (PI)	1	0	0	1	1
Peak 1 Mean by Intensity ordered by area (nm)	144.711	16.343	11.293	127.721	160.319
Peak 1 Area by Intensity ordered by area (%)	100	0	0	100	100

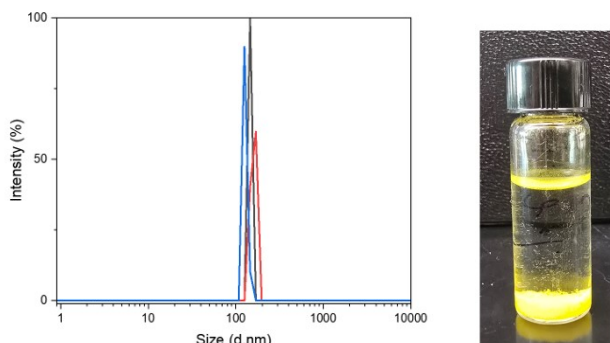


Figure S23: DLS of **2** (5.0 mM) in CH<sub>3</sub>CN and picture showing aggregation.

### Cyclic Voltammetry

The CV of both ligand and complex shows two reversible reduction waves corresponding to the formation of radical anion and dianions. However, reduction waves of ligand ( $E_{1/2} = -0.87$  and  $-1.25$  V vs Fc/Fc<sup>+</sup>) is more negative ( $E_{1/2} = -0.82$  and  $-1.18$  V vs Fc/Fc<sup>+</sup>) than complex i.e. upon platinum coordination, both reduction waves are shifted by about ~70 mV with respect to the ligand. This indicates the complex is easily reducible as it becomes electron deficient than ligand after coordination with the platinum ion. The platinum corners are not involved in the redox process within the applied potential range.

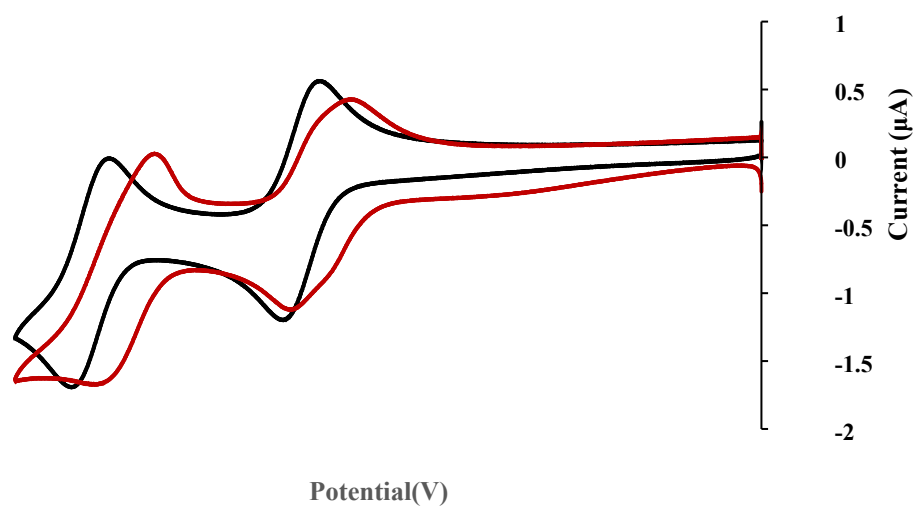


Figure S24: Cyclic Voltammetry of **1** (100  $\mu\text{M}$ ) and **2** (100  $\mu\text{M}$ ) in  $\text{CH}_2\text{Cl}_2$  at a gold electrode (0.05 M TBAP,  $\text{Ag}/\text{AgNO}_3$ , 100  $\text{mV}\cdot\text{s}^{-1}$ ).

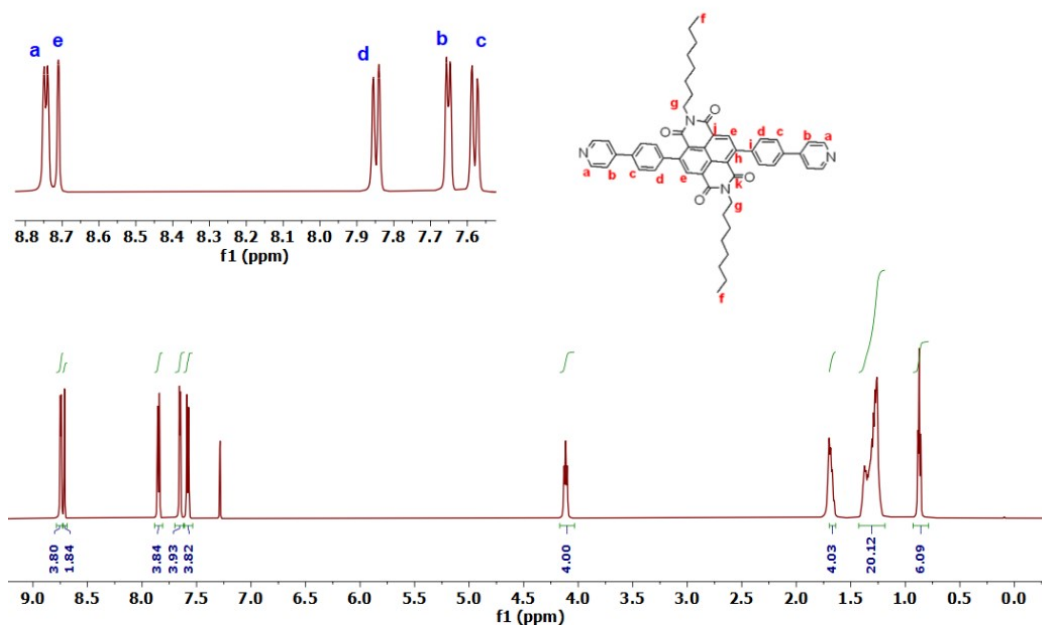


Figure S25 :  $^1\text{H}$  NMR of **1** in  $\text{CDCl}_3$ .

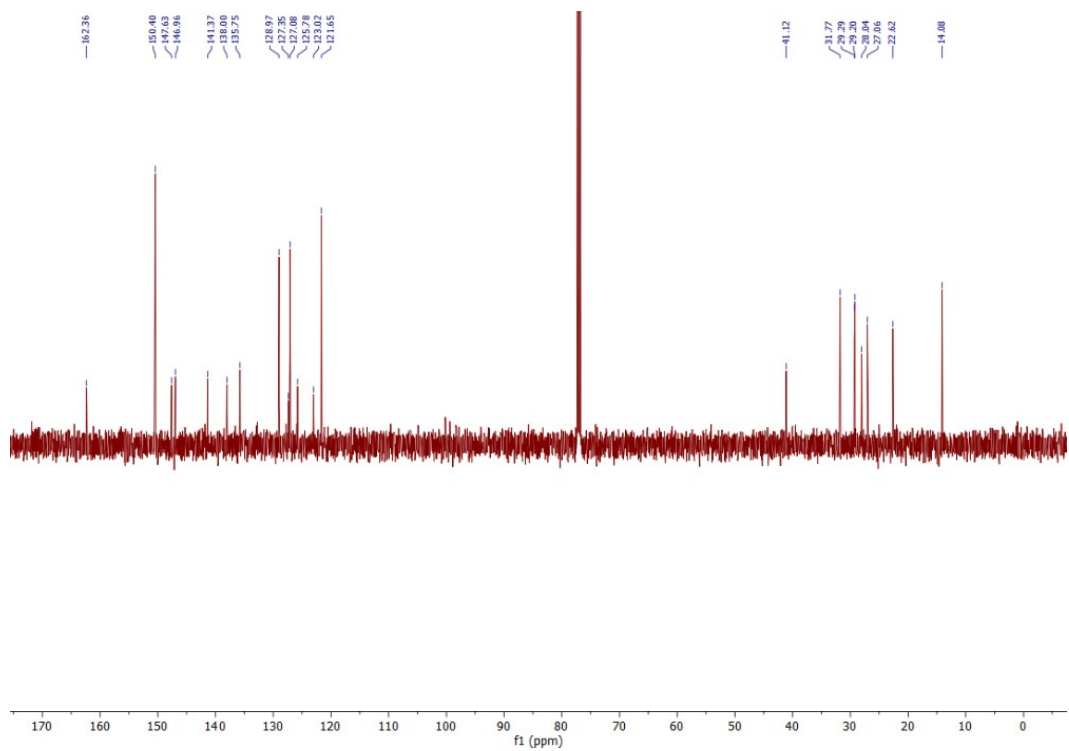


Figure S26:  $^{13}\text{C}$  NMR of **1** in  $\text{CDCl}_3$ .

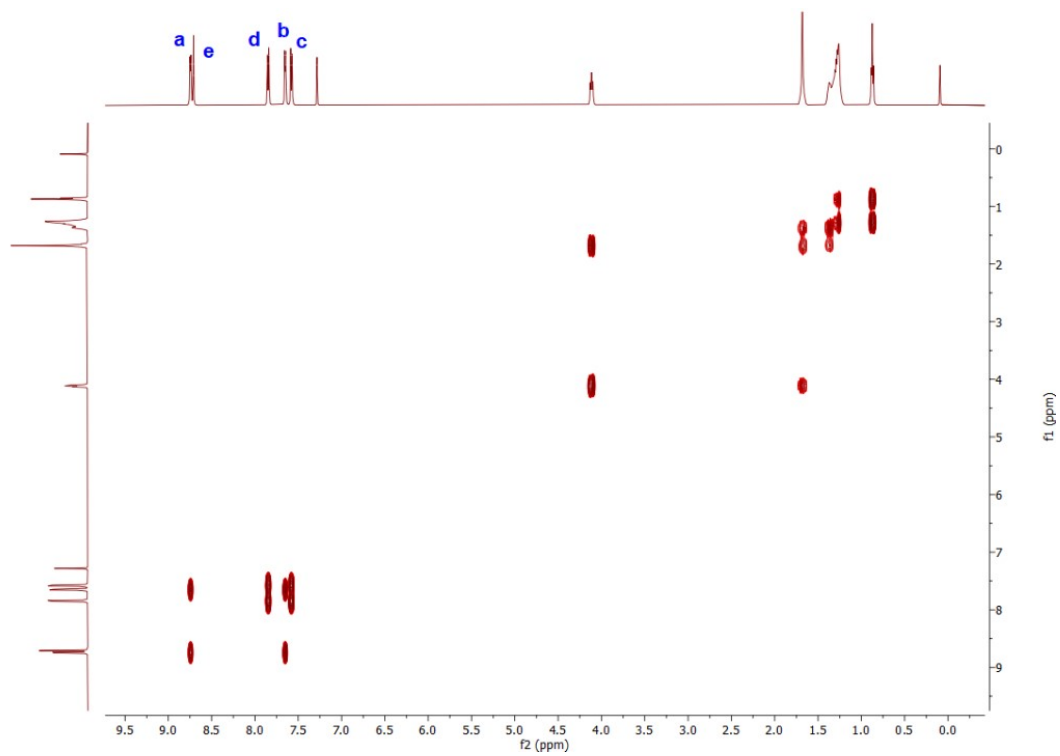


Figure S27: COSY of **1** in  $\text{CDCl}_3$ .

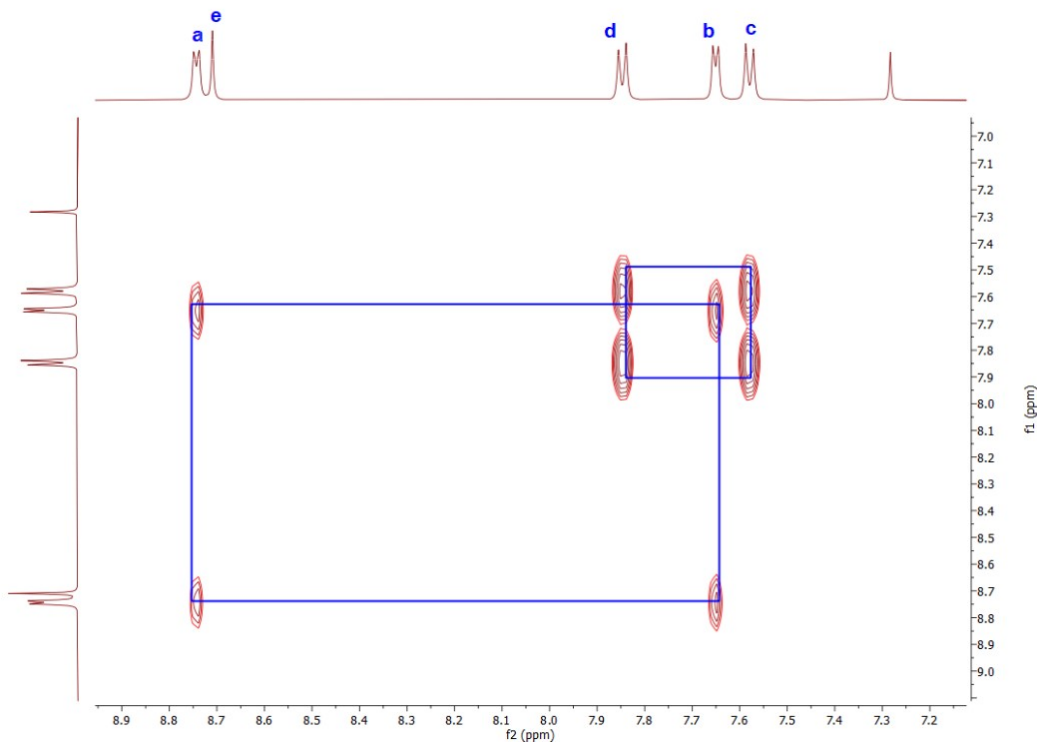


Figure S28: COSY (aromatic) of **1** in CDCl<sub>3</sub>.

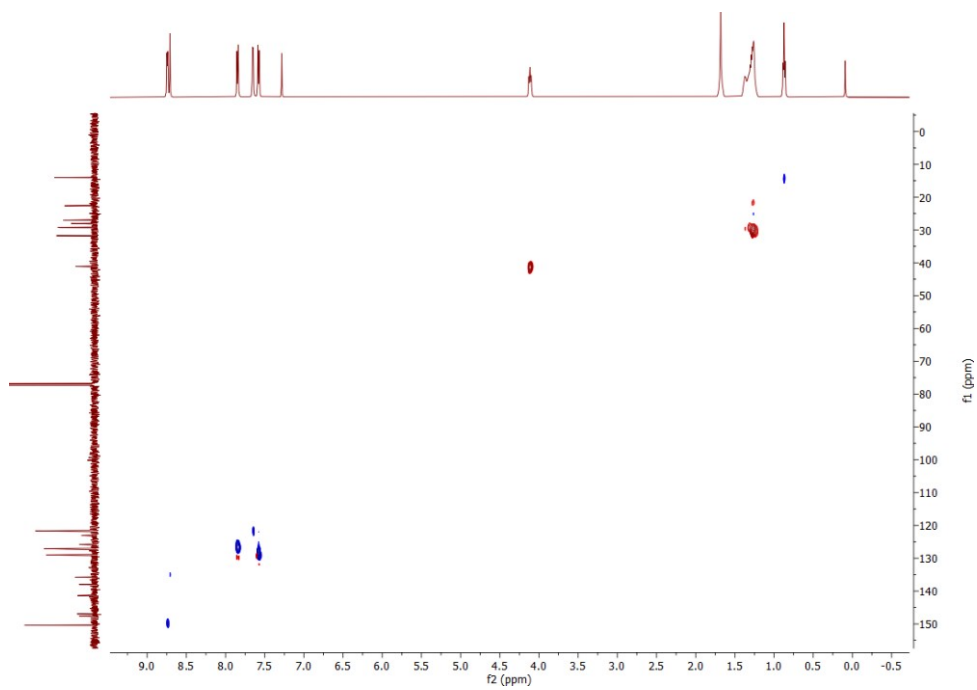


Figure S29: HSQC of **1** in CDCl<sub>3</sub>.

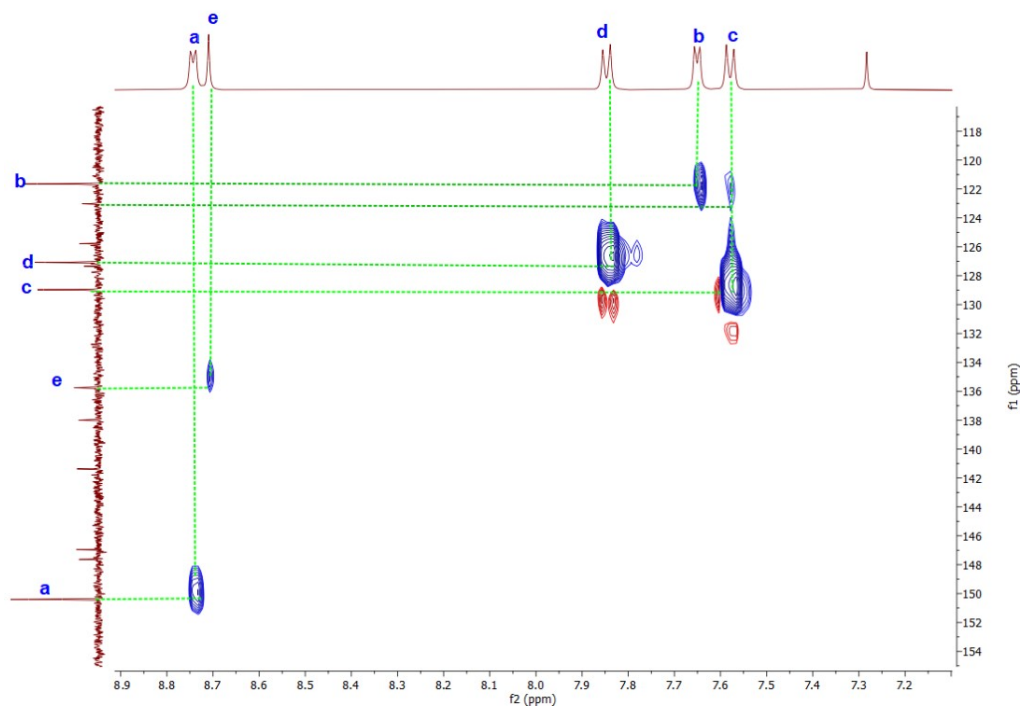


Figure S30: HSQC(aromatic) of **1** in CDCl<sub>3</sub>.

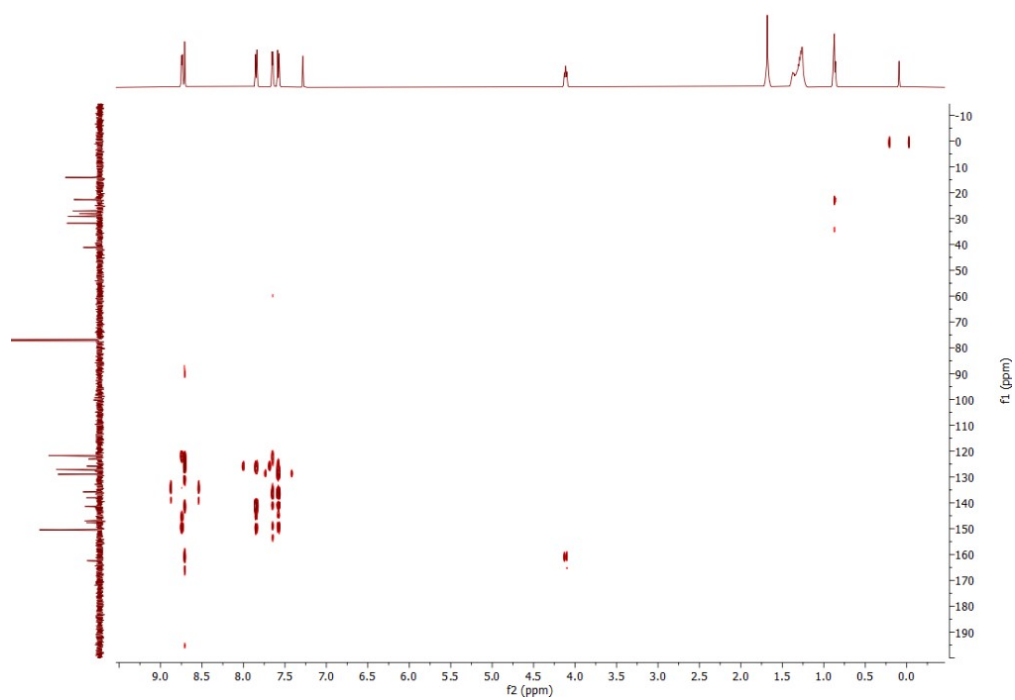


Figure S31: HMBC of **1** in CDCl<sub>3</sub>.

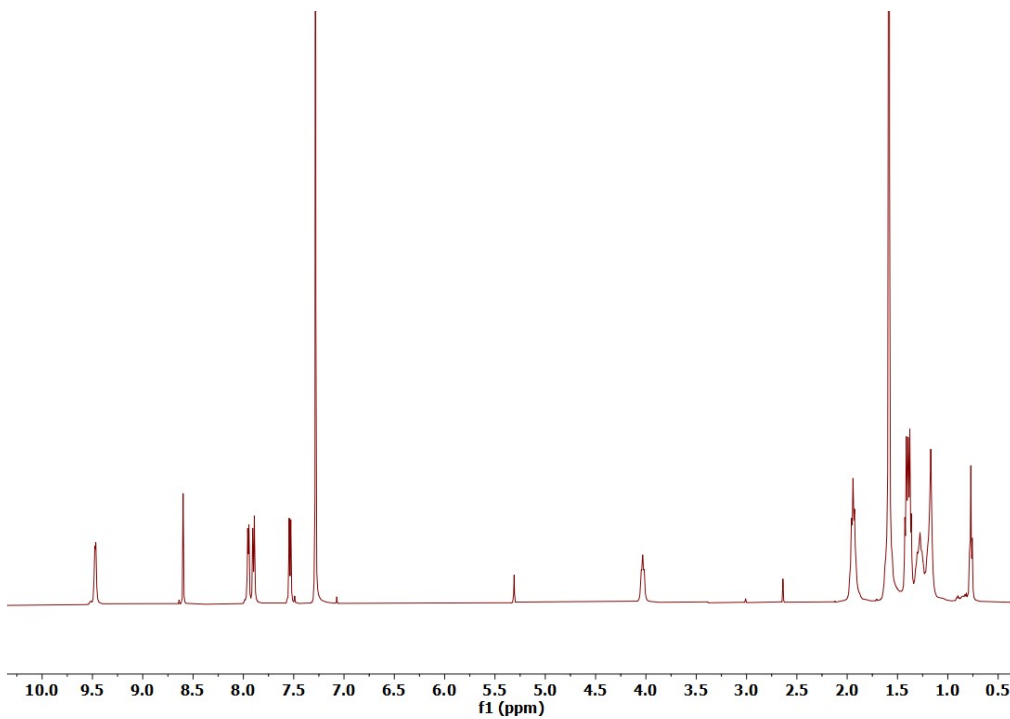


Figure S32:  $^1\text{H}$  NMR of **2** in  $\text{CDCl}_3$ .

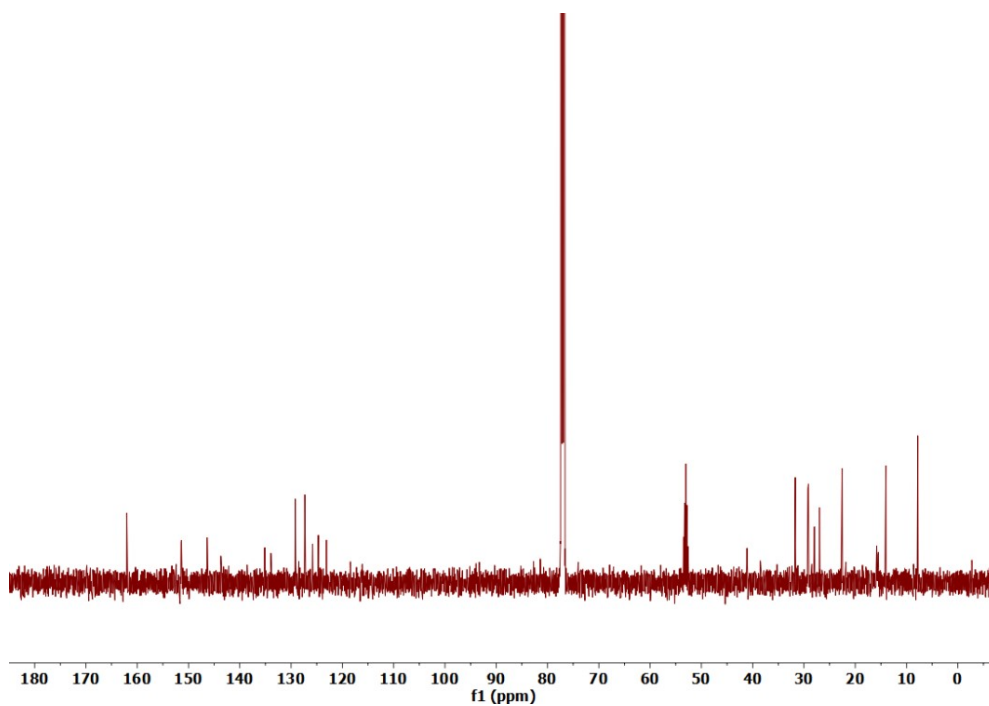


Figure S33:  $^{13}\text{C}$  NMR of **2** in  $\text{CDCl}_3$ .

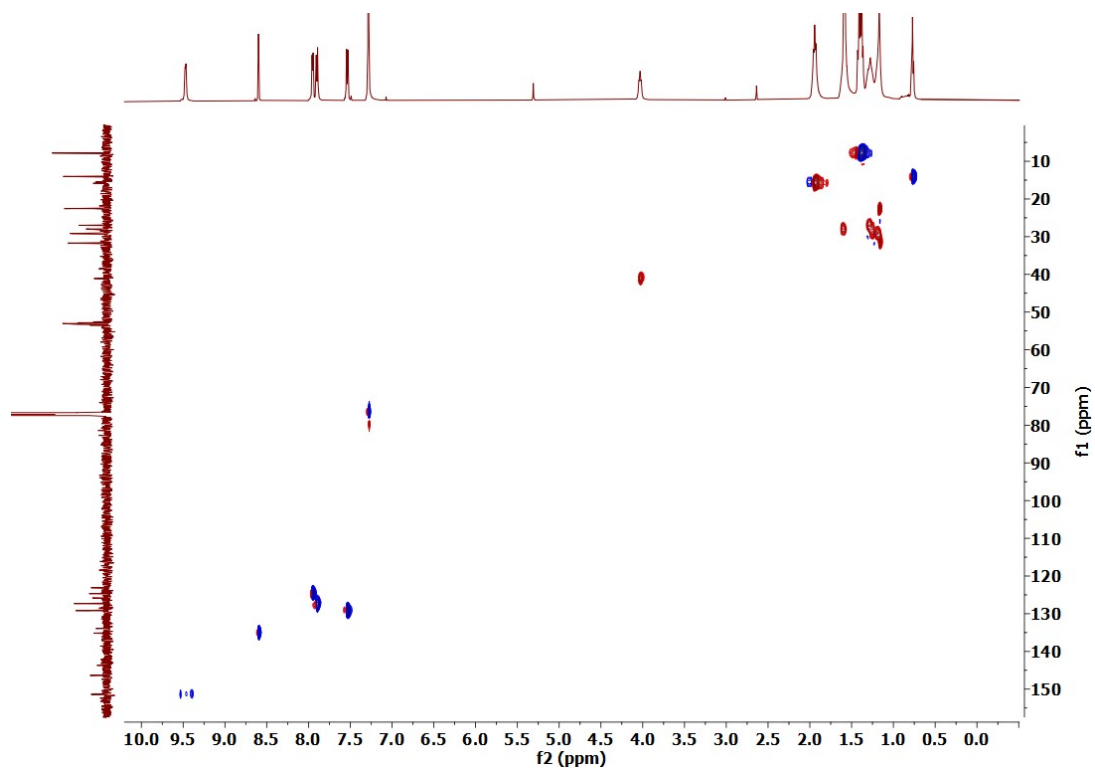


Figure S34: HSQC of **2** in  $\text{CDCl}_3$ .

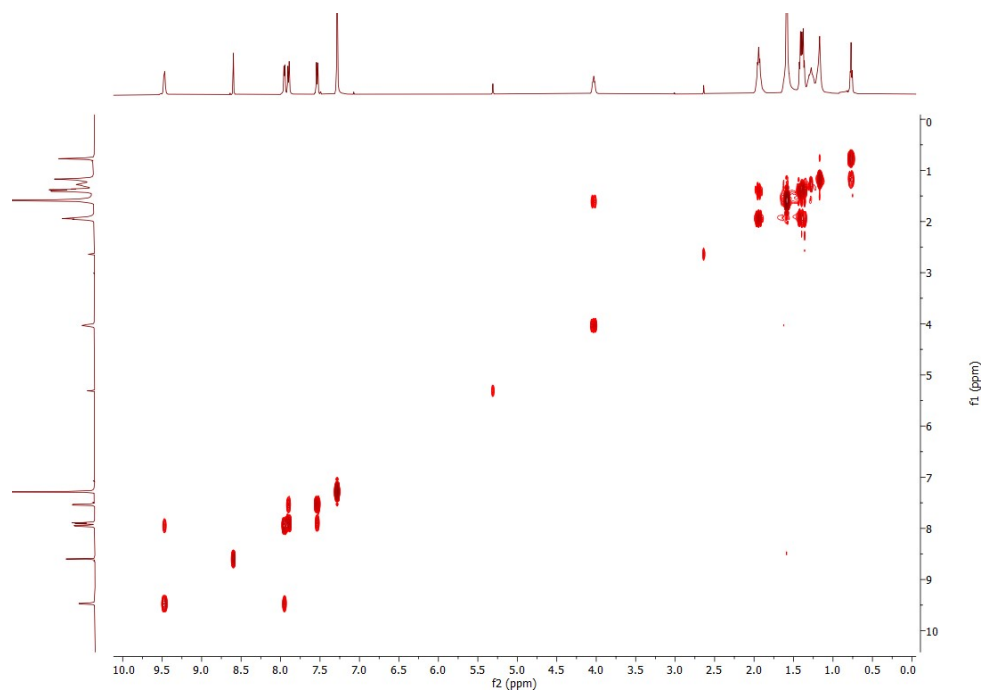


Figure S35: COSY of **2** in  $\text{CDCl}_3$ .

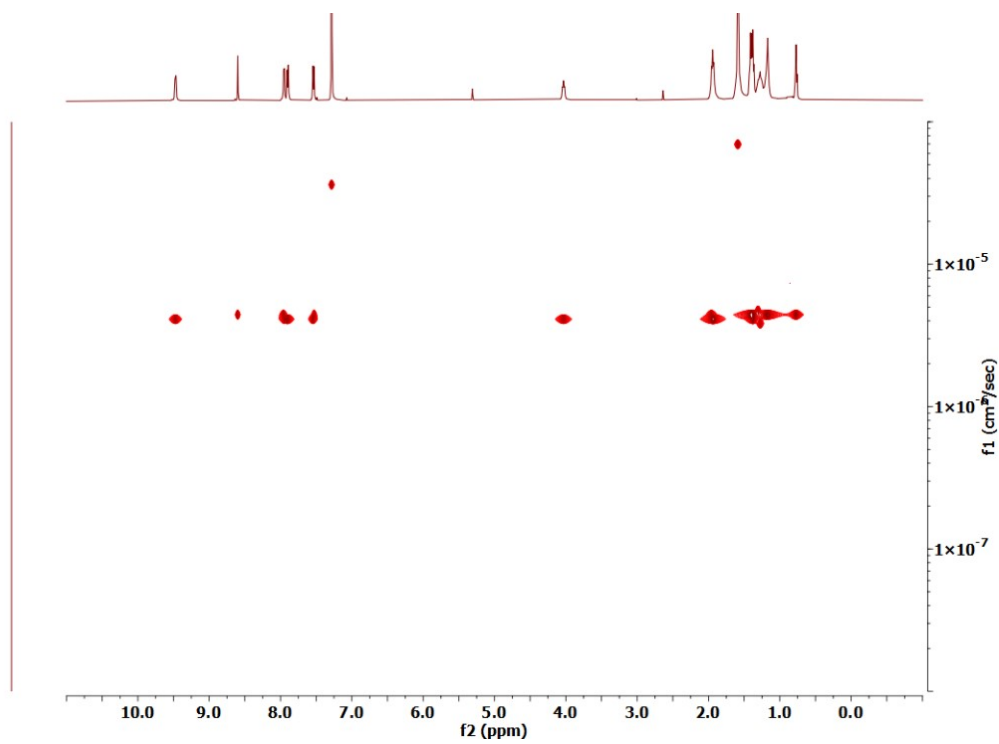


Figure S36: DOSY of **2** in CDCl<sub>3</sub>.

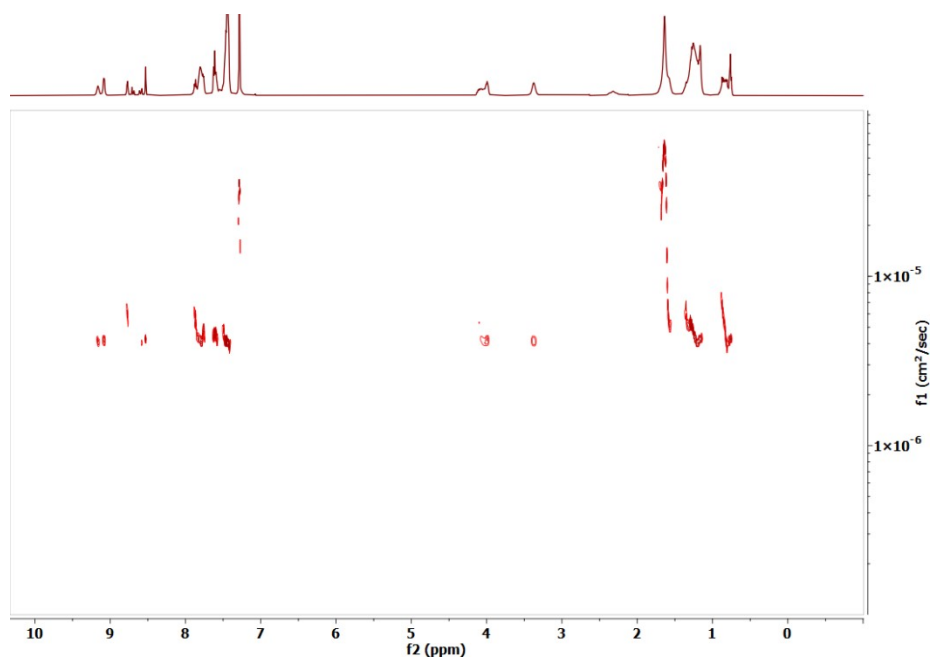


Figure S37: DOSY of **1** with Pt(dppp).2OTf in CDCl<sub>3</sub>.

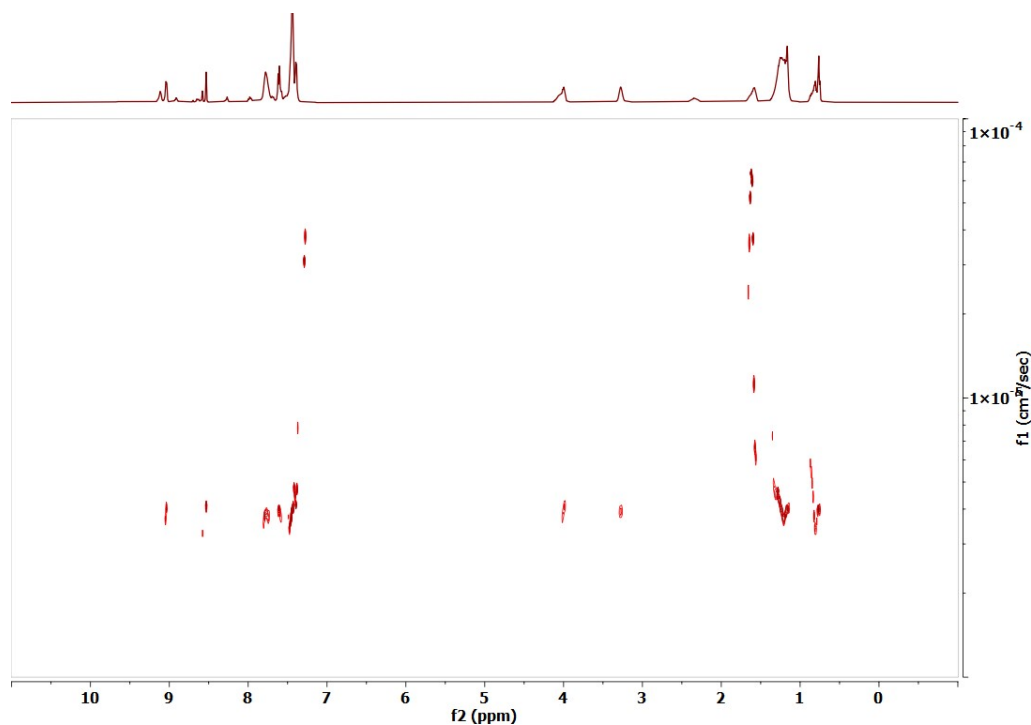


Figure S38: DOSY of **1** with Pd(dppp).2OTf in CDCl<sub>3</sub>.

- 1.M. Sasikumar, Y. V. Suseela and T. Govindaraju, *Asian Journal of Organic Chemistry*, 2013, **2**, 779-785.
- 2.Q. Sun, L. Escobar and P. Ballester, *Angewandte Chemie International Edition*, 2022, **61**, e202202140.
- 3.P. J. Stang, D. H. Cao, S. Saito and A. M. Arif, *Journal of the American Chemical Society*, 1995, **117**, 6273-6283.
- 4.Y. Yao, S. Chakraborty, S. Zhu, K. J. Endres, T.-Z. Xie, W. Hong, E. Manandhar, C. N. Moorefield, C. Wesdemiotis and G. R. Newkome, *Chemical Communications*, 2017, **53**, 8038-8041.
- 5.Spartan '24, *Journal*, **Wavefunction Inc. Irvine, CA 92612, USA**.
- 6.M. R. Sambrook, J. C. Vincent, J. A. Ede, I. A. Gass and P. J. Cragg, *RSC Advances*, 2017, **7**, 38069-38076.
- 7.J. Panidi, J. Kainth, A. F. Paterson, S. Wang, L. Tsetseris, A.-H. Emwas, M. A. McLachlan, M. Heeney and T. D. Anthopoulos, *Advanced Functional Materials*, 2019, **29**, 1902784.